

Dissipative fluid dynamics for the dilute Fermi gas at unitarity: Free expansion and rotation

T. Schäfer

Department of Physics, North Carolina State University, Raleigh, NC 27695

Abstract

We investigate the expansion dynamics of a dilute Fermi gas at unitarity in the context of dissipative fluid dynamics. Our aim is to quantify the effects of shear viscosity on the time evolution of the system. We compare exact numerical solutions of the equations of viscous hydrodynamics to various approximations that have been proposed in the literature. Our main findings are: i) Shear viscosity leads to characteristic features in the expansion dynamics; ii) a quantitative description of these effects has to include reheating; iii) dissipative effects are not sensitive to the equation of state $P(n, T)$ as long as the universal relation $P = \frac{2}{3}\mathcal{E}$ is satisfied; iv) the expansion dynamics mainly constrains the cloud average of the shear viscosity.

I. INTRODUCTION

A cold, dilute Fermi gas in which the scattering length can be tuned to infinity by means of a Feshbach resonance provides a new realization of a strongly correlated quantum fluid [1–3]. On resonance the two-body scattering amplitude saturates the s-wave unitarity bound, and the corresponding many-body system is referred to as the Fermi gas at unitarity. An important manifestation of strong correlations is the observation of nearly ideal hydrodynamic flow [4]. In the Fermi gas at unitarity nearly ideal flow was observed in samples containing as few as 10^5 atoms, with an interparticle spacing between the atoms on the order of several 10^3 \AA , much larger than the range of the interaction.

This result implies that dissipative effects must be very small [5]. In a normal fluid dissipative phenomena are governed by three transport coefficients, the shear viscosity η , the bulk viscosity ζ , and the thermal conductivity κ . The Fermi gas at unitarity is scale invariant and the bulk viscosity is zero [6, 7]. Most of the experiments conducted so far, like collective oscillations and the expansion from a deformed trap, involve scaling flows. In these flows the cloud remains nearly isothermal and the experiment is not sensitive to thermal conductivity [8, 9]. The observation of nearly ideal flow therefore requires that the shear viscosity is very small.

From a theoretical point of view we know that the shear viscosity of a weakly interacting gas scales as $\eta \sim \bar{p}/\sigma$, where \bar{p} is the mean momentum and σ is the scattering cross section. This implies that the shear viscosity of a strongly interacting gas is expected to be small. At unitarity the cross section is $\sigma = 4\pi/k^2$, where k is the momentum transfer. The average cross section in a thermal gas is $\sigma \simeq \frac{4\pi}{3}mT$, and the shear viscosity is $\eta \simeq \frac{15}{32\sqrt{\pi}}(mT)^{3/2}$ [10, 11]. This result is reliable as long as T is much larger than the critical temperature T_c for superfluidity. Below T_c the nature of the excitations changes and $\eta \sim 1/T^5$ [12]. These results indicate that the shear viscosity has a minimum at a temperature on the order of T_c , but kinetic theory cannot reliably predict how small the minimum value of the shear viscosity is. The region near T_c can be studied using sum rules [13], or with the help Kubo's formula and many body perturbation theory [14].

It has been argued that the quantum mechanical uncertainty relation implies a lower bound $\eta/n \sim \bar{p}l_{mfp} \geq \hbar$ [15]. Here, n is the density, $l_{mfp} \sim 1/(n\sigma)$ is the mean free path, and \hbar is Planck's constant. A more precise bound has emerged from the study of holographic

dualities in string theory. Kovtun, Son, and Starinets proposed that the shear viscosity to entropy density ratio η/s is bounded from below by $\hbar/(4\pi k_B)$ [16], where k_B is Boltzmann's constant.

Simple estimates of the shear viscosity to entropy density ratio based on experimental data indicate that η/s in the unitary Fermi gas is indeed close to the proposed bound. The first attempt to determine η/s from data was based on the damping of collective modes [17–19]. The damping constant can be related to the ratio \dot{E}/E , where E is the total energy of the mode and \dot{E} is the energy dissipated by viscous effects. For a scaling flow \dot{E} is proportional to the spatial integral of the shear viscosity. It was found that the ratio of the trap averages of η and s has a minimum value of $\langle\eta\rangle/\langle s\rangle \simeq 0.5$ [18, 19], where we have set $\hbar = k_B = 1$.

More recent analyses are based on the dynamics of an expanding cloud [8, 20–22]. These studies utilize approximate solutions of the equations of dissipative hydrodynamics. The first approximation is that entropy is assumed to be conserved, which is equivalent to the assumption that the system is in contact with an energy sink that removes the heat generated by dissipative effects. The second approximation is that the Navier-Stokes equation is converted into a set of ordinary differential equations by taking moments. If only the lowest moments are included then the result is only sensitive to the spatial integral of the shear viscosity. An analysis of the expansion of a rotating cloud gives values as small as $\langle\eta\rangle/\langle s\rangle \simeq 0.2$ [22]. A more refined approximation was used in [23] to analyze the high temperature limit of the shear viscosity. We will describe this method in Sect. V.

The goal of our present work is to test these approximations by performing numerical studies of the equations of viscous hydrodynamics for an expanding cloud of a dilute Fermi gas at unitarity. This paper is structured as follows. In Sect. II and III we introduce the equations of dissipative hydrodynamics for a scale invariant non-relativistic fluid. We discuss exact solutions for the ideal case and approximate solutions for the viscous case in Sects. IV and V. Numerical solutions are discussed in Sect. VI and our conclusions are summarized in Sect. VII.

II. DISSIPATIVE HYDRODYNAMICS

We will consider the unitary Fermi gas in the normal phase. In that case there are five hydrodynamic variables, the mass density ρ , the flow velocity \vec{v} , and the energy density \mathcal{E} . These variables satisfy four hydrodynamic equations, the continuity equation, the Navier-Stokes equation, and the equation of energy conservation,

$$\frac{\partial \rho}{\partial t} + \vec{\nabla} \cdot (\rho \vec{v}) = 0, \quad (1)$$

$$\frac{\partial(\rho v_i)}{\partial t} + \nabla_j \Pi_{ij} = 0, \quad (2)$$

$$\frac{\partial \mathcal{E}}{\partial t} + \vec{\nabla} \cdot \vec{j}^\epsilon = 0. \quad (3)$$

The total energy density is the sum of the internal energy density and kinetic energy density, $\mathcal{E} = \mathcal{E}_0 + \frac{1}{2}\rho v^2$. These equations close once we supply constitutive relations for the stress tensor Π_{ij} and the energy current j_i^ϵ as well as an equation of state. The unitary Fermi gas is scale invariant and the equation of state is $P = \frac{2}{3}\mathcal{E}_0$. The stress tensor is given by

$$\Pi_{ij} = \rho v_i v_j + P \delta_{ij} + \delta \Pi_{ij}, \quad (4)$$

where $\delta \Pi_{ij}$ is the dissipative part. The dissipative contribution to the stress tensor is $\delta \Pi_{ij} = -\eta \sigma_{ij}$ with

$$\sigma_{ij} = \left(\nabla_i v_j + \nabla_j v_i - \frac{2}{3} \delta_{ij} (\nabla_k v_k) \right), \quad (5)$$

where η is the shear viscosity and we have used the fact that the bulk viscosity of the unitary Fermi gas is zero. The energy current is

$$j_i^\epsilon = v_i w + \delta j_i^\epsilon, \quad (6)$$

where $w = \mathcal{E}_0 + P$ is the enthalpy density. The dissipative energy current is

$$\delta j_i^\epsilon = \delta \Pi_{ij} v_j - \kappa \nabla_i T, \quad (7)$$

where T is the temperature and κ is the thermal conductivity. We note that the temperature $T = T(n, P)$ is a function of the density $n = \rho/m$ and the pressure. In order to determine T we need the equation of state in the form $P = P(n, T)$. Universality implies that $P(n, T) = m^{-1} n^{5/3} f_n(mT/n^{2/3})$ where $f_n(x)$ is a universal function that has to be determined experimentally or using quantum Monte Carlo methods. The situation simplifies

in the high temperature limit where $P = nT$. We provide a parameterization of $P(n, T)$ at all temperatures in Appendix A. Universality also restricts the dependence of the shear viscosity and thermal conductivity on the density and the temperature. We can write

$$\eta(n, T) = \alpha_n \left(\frac{mT}{n^{2/3}} \right) n, \quad \kappa(n, T) = \sigma_n \left(\frac{mT}{n^{2/3}} \right) \frac{n}{m}, \quad (8)$$

where $\alpha_n(y)$ and $\sigma_n(y)$ are universal functions of $y = mT/n^{2/3}$. The relative importance of thermal and momentum diffusion can be characterized in terms of a dimensionless ratio known as the Prandtl number, $Pr = c_p \eta / (\rho \kappa)$, where c_p is the specific heat at constant pressure. In the high temperature limit $c_p = \rho/m$ and $Pr = \alpha_n / \sigma_n$. Kinetic theory predicts that in this limit $Pr = 2/3$ [9].

III. INITIAL CONDITIONS AND CHOICE OF UNITS

We will consider the expansion of a dilute Fermi gas after release from a harmonic trap. The density distribution in the initial state satisfies the equation of hydrostatic equilibrium, $\vec{\nabla} P = -n \vec{\nabla} V$, where $V(x) = \frac{1}{2} m \omega_i^2 x_i^2$ is the trapping potential. If the gas is isothermal then this equation is solved by the local density approximation

$$n_0(x) = n(\mu(x), T), \quad \mu(x) = \mu - V(x), \quad (9)$$

where $n(\mu, T)$ is the density in thermal equilibrium. The function $n(\mu, T)$ can be determined from the equation of state as explained in appendix A. The simplest case is the high temperature limit. In this limit the initial density is a Gaussian

$$n_0(x) = n_0 \exp \left(- \sum_i \frac{x_i^2}{R_i^2} \right), \quad (10)$$

with $R_i^2 = (2T)/(m\omega_i^2)$ and $n_0 = N/(\pi^{3/2} R_x R_y R_z)$. The total number of particles is denoted by N . In the following we will use a dimensionless coordinate variable $\bar{x}_i = x_i/x_0$ where

$$x_0^2 = \frac{2}{3m} \left(\frac{3N}{\omega_x \omega_y \omega_z} \right)^{1/3}. \quad (11)$$

This variable can be used for any initial condition, not just the Gaussian initial condition given in equ. (10). We will focus on axially symmetric traps with $\omega_x = \omega_y = \omega_\perp$ and $\omega_z = \lambda \omega_\perp$. In the high temperature limit the dimensionless density $\bar{n} = n x_0^3$ is given by

$$\bar{n}_0(\bar{x}) = \bar{n}_0 \exp \left(- \frac{E_F}{E_0} (\bar{x}^2 + \bar{y}^2 + \lambda^2 \bar{z}^2) \right), \quad (12)$$

where E_0 is the total (potential and internal) energy of the trapped gas and $E_F = (3N\lambda)^{1/3}N\omega_\perp$. The central density is $\bar{n}_0 = \lambda N(E_F/E_0)^{3/2}/\pi^{3/2}$.

We can write the equations of hydrodynamics in dimensionless variables by introducing a scaled time variable $\bar{t} = \omega_\perp t$ as well as a scaled velocity, energy density, and pressure,

$$\bar{v}_i = \frac{v_i}{x_0\omega_\perp}, \quad \bar{\mathcal{E}} = \frac{x_0}{m\omega_\perp^2} \mathcal{E}, \quad \bar{P} = \frac{x_0}{m\omega_\perp^2} P. \quad (13)$$

The scaled mass density is $\bar{\rho} = \rho x_0^3/m$. Using these variables the equations of fluid dynamics, equ. (1-3), remain unchanged except for the change from dimensionful to dimensionless hydrodynamic variables. The dimensionless shear viscosity is $\bar{\eta} = x_0\eta/(m\omega_\perp)$. We can write $\bar{\eta} = \bar{\alpha}_n\bar{n}$ with

$$\bar{\alpha}_n = \frac{3}{2} \frac{1}{(3\lambda N)^{1/3}} \alpha_n, \quad (14)$$

where α_n is the universal function introduced in equ. (8). Finally, we can introduce a dimensionless temperature and chemical potential, $\bar{T} = T/(m\omega_\perp^2 x_0^2)$ and $\bar{\mu} = \mu/(m\omega_\perp^2 x_0^2)$.

IV. EXACT SOLUTIONS

In order to test the accuracy of the numerical hydrodynamics code we have studied a number of exactly solvable test cases. In ideal hydrodynamics there are exact scaling solutions for the expansion from rotating and non-rotating traps. Consider a density profile of the form

$$n(x, t) = \frac{1}{b_x(t)b_y(t)b_z(t)} F\left(\frac{x^2}{b_x^2(t)} + \frac{y^2}{b_y^2(t)} + \frac{\lambda^2 z^2}{b_z^2(t)}\right), \quad (15)$$

where $F(x)$ is an arbitrary function and the scale parameters $b_i(t)$ satisfy the initial condition $b_i(0) = 1$. This ansatz satisfies the continuity equation with a velocity field given by $v_i(x, t) = \alpha_i(t)x_i$ with $\alpha_i = \dot{b}_i/b_i$. The initial condition for the pressure can be determined by integrating the equation of hydrostatic equilibrium

$$P_0(x) = - \int n_0(x) \vec{\nabla} V(x) \cdot d\vec{x}. \quad (16)$$

In the limit $T \gg T_F$ the function $F(x)$ is a Gaussian and the initial pressure is determined by the ideal gas equation of state, $P = nT$. In the initial state the temperature is constant and the chemical potential is parabolic. In ideal hydrodynamics the evolution of the system preserves these properties. The Gibbs-Duhem relation $dP = nd\mu + sdT$ implies that the force $(\vec{\nabla} P)/n = \vec{\nabla} \mu$ is exactly linear at all times.

The Euler equation is equivalent to three coupled ordinary differential equations for the scale parameters b_i . We get [8, 24]

$$\ddot{b}_i = \frac{\omega_i^2}{(b_x b_y b_z)^{2/3} b_i}, \quad (17)$$

with the initial conditions $b_i(0) = 1$ and $\dot{b}_i(0) = 0$. In the case of axial symmetry this set of equations reduces to two independent equations for $b_\perp = b_x = b_y$ and b_z . These differential equations have to be solved numerically.

This solution can be generalized to an initial velocity field that corresponds to a rotating trap. The velocity field can be chosen to be irrotational, $\vec{v} = \alpha \vec{\nabla}(xz)$, or rigidly rotating, $\vec{v} = \Omega \hat{y} \times \vec{x}$. Here we have chosen the direction of the angular momentum to be in the y -direction. In the rotating case the profile function in equ. (15) has to be generalized to include an off-diagonal xz -term. In total one has to solve for ten functions, the four scale parameters b_x, b_y, b_z and b_{xz} , the chemical potential at the center of the trap, and five functions characterizing the velocity field, $\alpha_x, \alpha_y, \alpha_z, \alpha$ and Ω . The equations of motion are given in [8, 25].

There are no known exact solutions for an expanding gas in the dissipative case. However, we can find scaling solutions to the continuity and Navier-Stokes equation if the local shear viscosity is of the form $\eta = \eta_0 P/T$, where η_0 is a constant. Note that at high temperature $P = nT$ and $\eta = \eta_0 n$. Also, for any scaling solution $T = \text{const}$ and $\vec{\nabla}\eta = \eta_0(\vec{\nabla}P)/T$, which implies that both the ideal and the dissipative forces are proportional to the gradient of the pressure. The Navier-Stokes equation then leads to the coupled set of equations

$$\ddot{b}_\perp = \frac{\omega_\perp^2}{(b_\perp^2 b_z)^{2/3} b_\perp} - \frac{2\beta\omega_\perp}{b_\perp} \left(\frac{\dot{b}_\perp}{b_\perp} - \frac{\dot{b}_z}{b_z} \right) \quad (18)$$

$$\ddot{b}_z = \frac{\omega_z^2}{(b_\perp^2 b_z)^{2/3} b_z} + \frac{4\beta\lambda\omega_z}{b_z} \left(\frac{\dot{b}_\perp}{b_\perp} - \frac{\dot{b}_z}{b_z} \right), \quad (19)$$

where we have specialized the solution to the case of axial symmetry and we have defined $\beta = \eta_0\omega_\perp/(3T_0)$, where T_0 is the initial temperature. We can write the parameter β as

$$\beta = \frac{\langle \alpha_n \rangle}{(3N\lambda)^{1/3}} \frac{1}{(E_0/E_F)} = \frac{2}{3} \frac{\langle \bar{\alpha}_n \rangle}{(E_0/E_F)}, \quad (20)$$

where $\langle \alpha_n \rangle$ is the trap average of α_n ,

$$\langle \alpha_n \rangle = \frac{1}{N} \int d^3x \alpha_n \left(\frac{mT}{n_0(x)^{2/3}} \right) n_0(x), \quad (21)$$

and we have used equ. (14). The solution of equ. (18,19) does not conserve energy. Instead, it satisfies a modified energy equation

$$\frac{\partial \mathcal{E}}{\partial t} + \vec{\nabla} \cdot \vec{j}^e = -\frac{\eta}{2} (\sigma_{ij})^2, \quad (22)$$

which contains a sink that removes the heat generated by dissipative effects. This means that the scaling solution conserves entropy even if the shear viscosity is not zero. The produced entropy is removed by the heat sink. We also note that equ. (18,19) can be generalized to the rotating case, see [8].

V. VISCOUS HYDRODYNAMICS: APPROXIMATE SOLUTIONS

If dissipative effects are mostly governed by viscous forces, and reheating is not important, then the scaling solution introduced in the previous section is a useful approximation to the full hydrodynamic equations. We will show below that for an expanding system this is not the case. A more useful approximation was recently proposed in [23]. We will assume that the local shear viscosity is proportional to the density, $\eta = \alpha_n n$, where α_n is a constant. The basic idea is to focus on the force $f_i = (\nabla_i P)/n$ rather than the pressure itself. The Navier-Stokes equation is

$$m \left(\frac{\partial}{\partial t} + \vec{v} \cdot \vec{\nabla} \right) v_i = f_i + \frac{\nabla_j (\eta \sigma_{ij})}{n}. \quad (23)$$

With the help of the Navier-Stokes equation the energy equation can be written as

$$\left(\frac{\partial}{\partial t} + \mathbf{v} \cdot \nabla + \frac{2}{3} (\vec{\nabla} \cdot \vec{v}) \right) f_i + (\nabla_i v_j) f_j - \frac{5}{3} (\nabla_i \nabla_j v_j) \frac{P}{n} = -\frac{2}{3} \frac{\nabla_i \dot{q}}{n}, \quad (24)$$

where $\dot{q} = \frac{\eta}{2} (\sigma_{ij})^2$ is the heating rate. The basic idea is to assume that even in the dissipative case the velocity field and the force remain linear in the coordinates. If the velocity is linear and $\eta \sim n$ then all terms in equ. (23) are linear in x_i . Also, equ. (24) is independent of the pressure and all the remaining terms are linear in x_i . We write $f_i = a_i x_i$, $v_i = \alpha_i x_i$ (no sum over i) and use the scaling ansatz (15) for the density. The continuity equation requires $\alpha_i = \dot{b}_i / b_i$. The scale parameters a_i and b_i are determined by the coupled equations

$$\frac{\ddot{b}_\perp}{b_\perp} = a_\perp - \frac{2\beta\omega_\perp}{b_\perp^2} \left(\frac{\dot{b}_\perp}{b_\perp} - \frac{\dot{b}_x}{b_x} \right), \quad (25)$$

$$\frac{\ddot{b}_z}{b_z} = a_z + \frac{4\beta\lambda\omega_z}{b_z^2} \left(\frac{\dot{b}_\perp}{b_\perp} - \frac{\dot{b}_z}{b_z} \right), \quad (26)$$

$$\dot{a}_\perp = -\frac{2}{3} a_\perp \left(5 \frac{\dot{b}_\perp}{b_\perp} + \frac{\dot{b}_z}{b_z} \right) + \frac{8\beta\omega_\perp^2}{3b_\perp} \left(\frac{\dot{b}_\perp}{b_\perp} - \frac{\dot{b}_z}{b_z} \right)^2, \quad (27)$$

$$\dot{a}_z = -\frac{2}{3} a_z \left(4 \frac{\dot{b}_z}{b_z} + 2 \frac{\dot{b}_\perp}{b_\perp} \right) + \frac{8\beta\lambda\omega_z}{3b_z^2} \left(\frac{\dot{b}_\perp}{b_\perp} - \frac{\dot{b}_z}{b_z} \right)^2, \quad (28)$$

where β is defined in equ. (20). The initial conditions are $b_\perp(0) = b_z(0) = 1$, $\dot{b}_\perp(0) = \dot{b}_z(0) = 0$ as before, and $a_\perp(0) = \omega_\perp^2$, $a_z(0) = \omega_z^2$. We note that the solutions of equ. (25-28) provide an exact solution of the continuity, Navier-Stokes, and energy conservation equation. The solution is approximate in the sense that one cannot in general find a consistent expression for the pressure $P(\mu, T)$ such that P, \mathcal{E}, n are related by thermodynamic identities.

VI. VISCOUS HYDRODYNAMICS: NUMERICAL RESULTS

A. Numerical tests

Ideal hydrodynamic simulations were carried out using the VH1 code written by Blondin and Lufkin [26]. VH1 uses the PPMLR (Piecewise-Parabolic Method, Lagrangian-Remap) method developed by Colella and Woodward [27, 28]. The hydrodynamic equations are written in the form of conservation laws and solved in Lagrangian coordinates. A Lagrangian time step is followed by a piecewise parabolic remap onto an Eulerian grid. We have modified VH1 to include viscous corrections to the stress tensor and the energy current. In the current work we have not included the effect of thermal conductivity. In the ideal case the cloud remains isothermal during the expansion and $\vec{\nabla}T = 0$. Dissipative effects lead to non-zero temperature gradients, but if the viscosity and thermal conductivity are small then the corresponding correction to the energy current is second order in small quantities. We will verify this statement in Sect. VIB.

We first consider the evolution of a Gaussian density profile in ideal hydrodynamics. The initial condition is given by equ. (12) where we have chosen $E_0/E_F = 1$ and $\bar{n}_0 = 1$ (the ideal evolution is independent of the number of particles). The aspect ratio of the cloud is $\lambda = 0.045$. In Fig. 1 we show the evolution of the density and the velocity. The points are the results of the numerical solution using VH1 and the lines are semi-analytic results based on solving the coupled set of ordinary differential equations (17). The numerical calculation was performed on a fairly coarse grid with a grid spacing $\Delta\bar{x} = 0.2$. We observe that the numerical calculation is nevertheless very accurate.

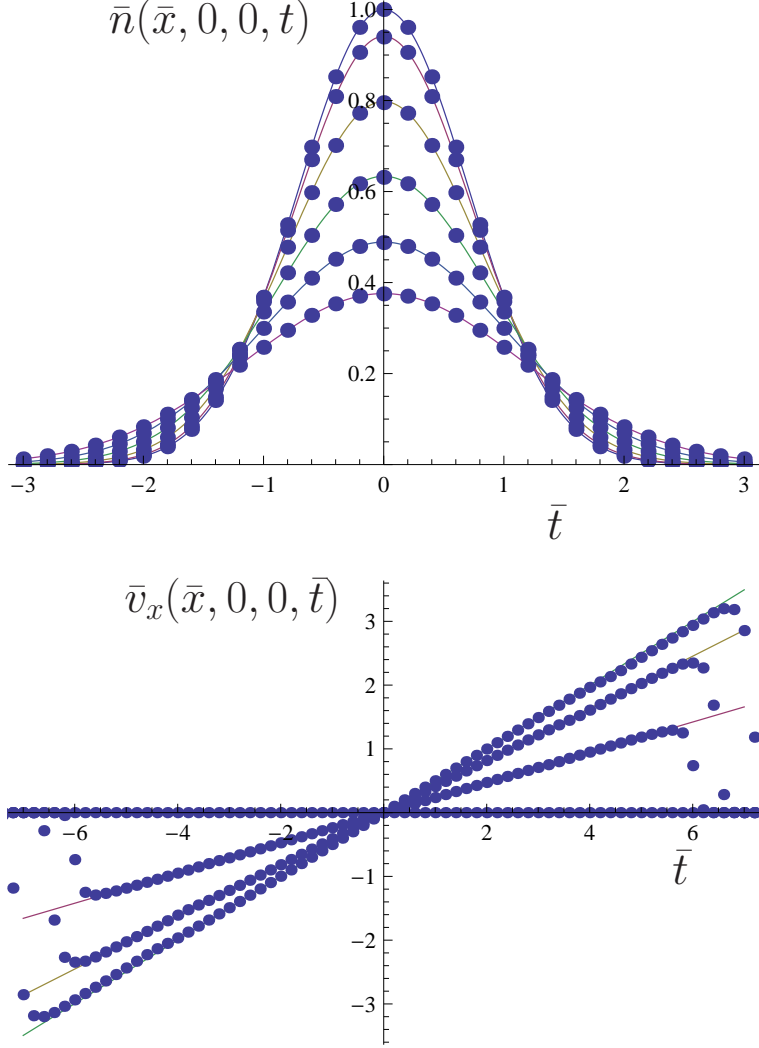


FIG. 1: Density and velocity profile of an expanding gas cloud in ideal hydrodynamics. The initial condition is a Gaussian density profile with $E_0/E_F = 1$. The top panel shows the density $\bar{n}(\bar{x}, 0, 0, \bar{t})$ for $\bar{t} = 0.0, 0.25, 0.50, \dots, 1.25$. The solid lines show the analytic solution of the Euler equation, and the dots show numerical results. The bottom panel shows the velocity $\bar{v}_x(\bar{x}, 0, 0, \bar{t})$ for $\bar{t} = 0.0, 0.25, 0.50, 0.75$.

The lower panel of Fig. 1 shows that the velocity field tracks the linear behavior of the analytic solution only up to some maximum distance which slowly grows with time. The turnover of the velocity field is related to the fact that we impose a minimum density and pressure (10^{-15} of the initial central density and pressure). Beyond the point at which the minimum pressure is reached there are no pressure gradients and therefore no acceleration. The sharp discontinuity in the velocity does not lead to numerical problems. A smooth

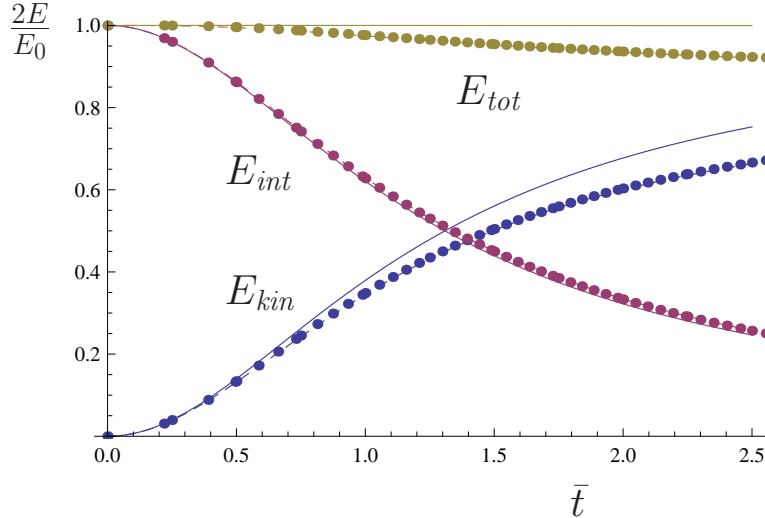


FIG. 2: Energy of the expanding gas cloud as a function of time. We show the kinetic, internal, and total energy. The solid lines show the analytical result for the ideal evolution, the dashed lines show the analytical result without reheating for $\beta = 0.066$, and the points are from a numerical calculation with $E_0/E_F = 1$ and $\bar{\eta} = \bar{\alpha}_n \bar{n}$ with $\bar{\alpha}_n = 0.1$. In the simulation we remove the heat generated by dissipative effects.

turnover of the velocity field can be achieved by considering slightly modified initial conditions. If we solve the equation of hydrostatic equilibrium in a potential which is harmonic at short distances, but grows as $V \sim |\vec{x}|^\alpha$ with $\alpha < 1$ at large distances, then the velocity field of the expanding cloud will go to zero smoothly as $|\vec{x}| \rightarrow \infty$.

We next consider the dissipative evolution of a Gaussian density profile. We take the shear viscosity to be of the form $\eta = \alpha_n n$ with a constant α_n . In order to compare with the solution discussed in Sect. IV we include a sink in the equation of energy conservation as defined in equ. (22). Note that we can write the divergence of the dissipative energy current as

$$\nabla_i(\delta j_i^\epsilon) = \nabla_i(v_j \delta \Pi_{ij}) = -\frac{\eta}{2}(\sigma_{ij})^2 + v_i \nabla_j \delta \Pi_{ij}. \quad (29)$$

The first term corresponds to viscous heating and the second term describes the work done by viscous forces. Adding a heat sink implies that we only keep the effect of the work term.

The evolution of the kinetic, potential, and total energy for $\bar{\alpha}_n = 0.1$ and $E_0/E_F = 1$ are shown in Fig. 2. The solid lines show the ideal evolution determined by equ. (17) and the dashed lines show the dissipative result given by the solution of equ. (18,19) for

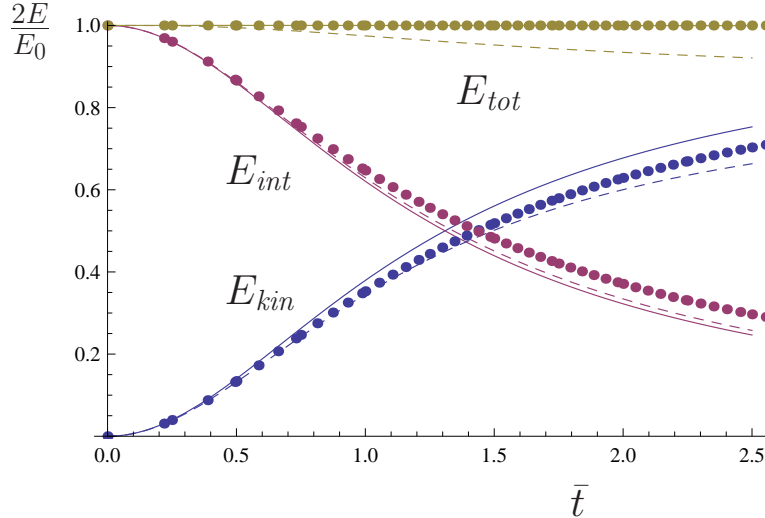


FIG. 3: Energy of the expanding gas cloud as a function of time. We show the kinetic, internal, and total energy. The solid lines show the analytical result for the ideal evolution, and the dashed lines show the analytical result without reheating for $\beta = 0.066$. The data points show the result of a numerical calculation with $E_0/E_F = 1$ and $\bar{\eta} = \bar{\alpha}_n \bar{n}$ with $\bar{\alpha}_n = 0.1$. The simulation includes all dissipative terms in the energy current.

$\beta = \frac{2}{3} \bar{\alpha}_n (E_F/E_0) = 0.066$. The data points come from a numerical calculation based on the dissipative version of VH1. We observe that the data agree very well with the analytical solution. The main difference between the dissipative and the ideal solution is that a fraction of the kinetic energy is converted to heat. The heat is absorbed by the sink and lost to the system. The evolution of the internal energy is only affected indirectly, via the effect of dissipation on the evolution of the radius of the system.

B. Effects of reheating

The evolution of the energy in a complete simulation, including the effects of reheating, is shown in Fig. 3. The system parameters are the same as in the previous section. We observe that the total energy is conserved to a very good accuracy. Reheating increases the internal energy as compared to the result in ideal hydrodynamics. Hydrodynamic evolution converts the added internal energy into kinetic energy. This implies that reheating leads to reacceleration.

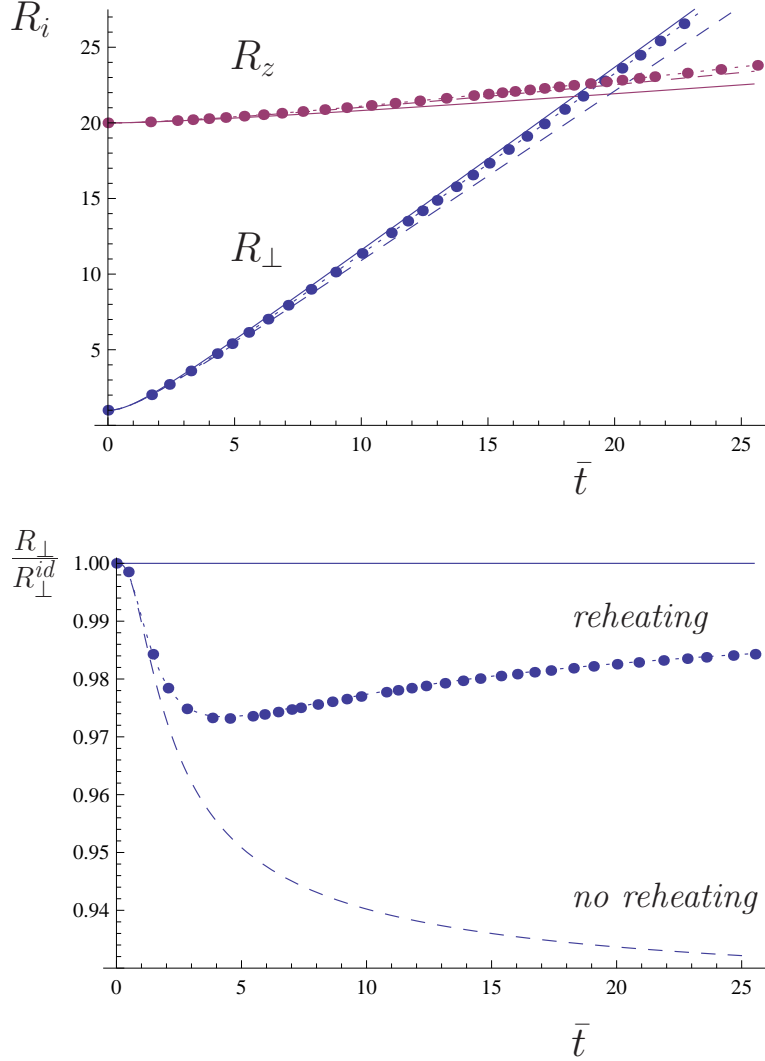


FIG. 4: The top panel shows the transverse and longitudinal scale factors of the expanding gas cloud as a function of time. The initial density has a Gaussian profile with $\lambda = 0.05$ and $E_0/E_F = 1$. The viscosity is of the form $\bar{\eta} = \bar{\alpha}_n \bar{n}$ with $\bar{\alpha}_n = 0.1$. The solid lines show the analytical result for the ideal evolution, the dashed lines correspond to the dissipative solution without reheating, and the dotted line is the approximate solution described in Sect. V. The points are from a numerical calculation. The bottom panel shows the ratio of the transverse scale factor over the result in ideal hydrodynamics for the calculations shown in the top panel.

This is shown in more detail in Fig. 4. The upper panel shows the time evolution of the Gaussian radii $R_{\perp}(t)$ and $R_z(t)$. We have normalized $R_{\perp}(0) = 1$ and $R_z(0) = 1/\lambda$ so that $R_{\perp}(T) = R_z(t)$ corresponds to an aspect ratio of one. The solid lines show the result

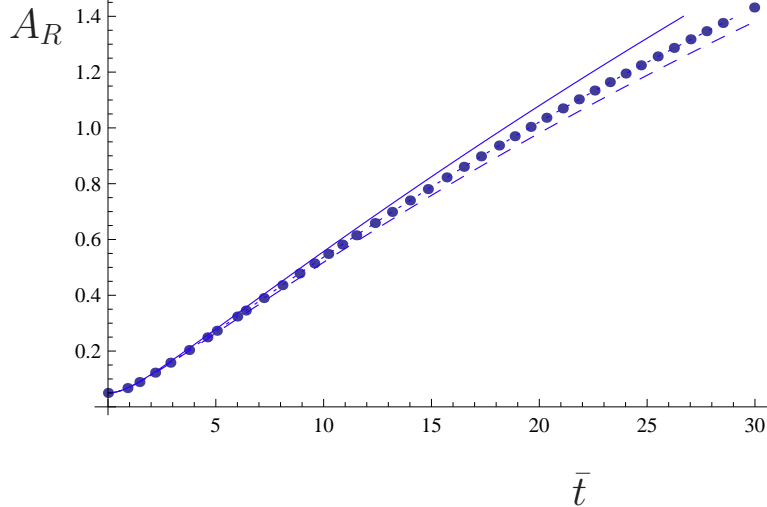


FIG. 5: This figure shows the time evolution of the aspect ratio $A_R = \lambda R_{\perp}(t)/R_z(t)$. The solid lines show the analytical result for the ideal evolution, the dashed lines correspond to the dissipative solution without reheating, and the dotted line is the approximate solution described in Sect. V. The points are from a numerical calculation. All curves correspond to a Gaussian initial condition, and the viscosity is of the form $\bar{\eta} = \bar{\alpha}_n \bar{n}$ with $\bar{\alpha}_n = 0.1$.

in ideal hydrodynamics, the dashed lines show the result without reheating, the dotted line shows the approximate solution including reheating discussed in Sect. V, and the data points are obtained from a numerical calculation. The lower panel shows the ratio $R_{\perp}(t)/R_{\perp}^{id}(t)$ where $R_{\perp}^{id}(t)$ is the transverse size in ideal hydrodynamics. We observe that the two radii initially track the prediction of the calculation without reheating: Viscosity slows down the expansion in the short direction, and accelerates the system in the longitudinal direction. At later times reheating leads to an acceleration in both directions. The lower panel of Fig. 4 shows that the transverse size almost goes back to the prediction of ideal hydrodynamics. For a shear viscosity which is linear in the density this behavior is very well described by the linear force model discussed in Sect. V.

Fig. 5 shows that even if reheating is taken into account shear viscosity leads to significant effects in the evolution of the aspect ratio $A_R = \lambda R_{\perp}/R_z$. The shape of $A_R(t)$ is similar in the model without reheating and the numerical simulation, but the magnitude of the dissipative effect is about a factor 2 smaller if reheating is taken into account. We observe that shear viscosity leads to a characteristic bending of $A_R(t)$ in the regime $A_R \sim 1$. In ideal

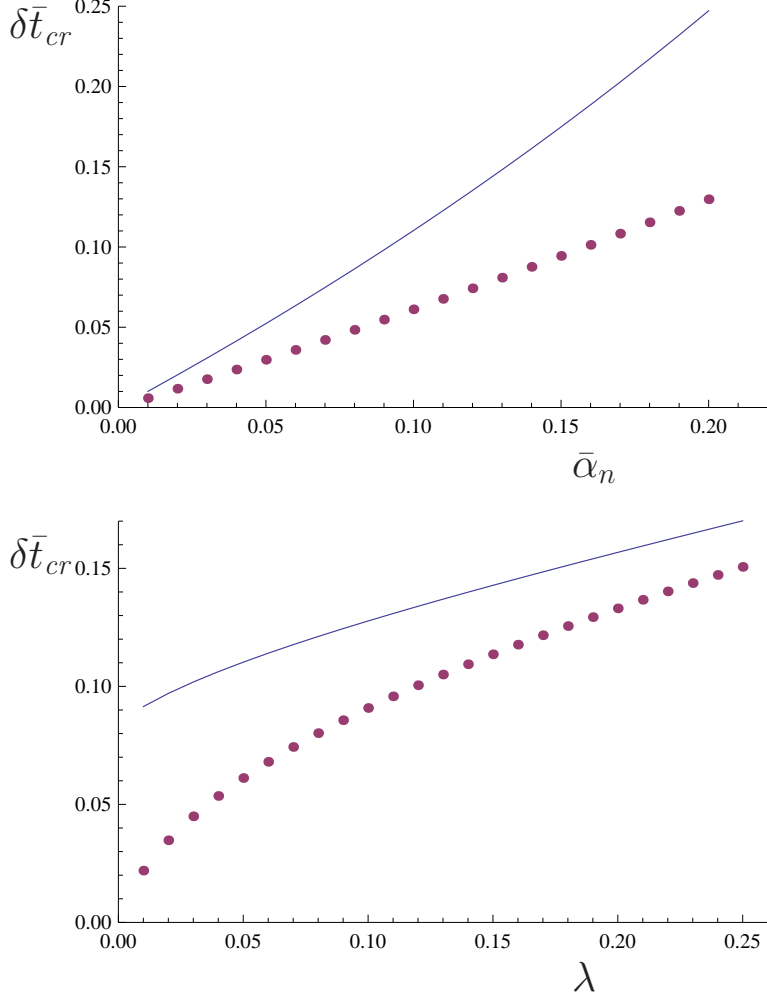


FIG. 6: This figure shows the viscous correction to the crossing time t_{cr} defined by $A_R(t_{cr}) \equiv 1$. The top panel shows $\delta \bar{t}_{cr}$ as a function of the viscosity $\bar{\alpha}_n$, where $\bar{\eta} = \bar{\alpha}_n \bar{n}$, for $E_0/E_F = 1$ and a fixed initial aspect ratio $\lambda = 0.05$. The solid line is the result of the dissipative calculation without reheating and the points are from a numerical calculation. The bottom panel shows $\delta \bar{t}_{cr}$ as a function of λ for a fixed viscosity $\bar{\alpha}_n = 0.1$

hydrodynamics acceleration takes place at early times $\bar{t} \lesssim 3$. Dissipative forces and reheating lead to longitudinal acceleration which occurs on a much longer time scale. Observing this behavior not only constrains the value of the shear viscosity, it also demonstrates that the systems continues to behave hydrodynamically even at very late times.

The effect of shear viscosity on the evolution of $A_R(t)$ can be quantified in terms of the “crossing time” t_{cr} defined by $A_R(t_{cr}) \equiv 1$. Viscosity leads to a shift δt_{cr} in the crossing

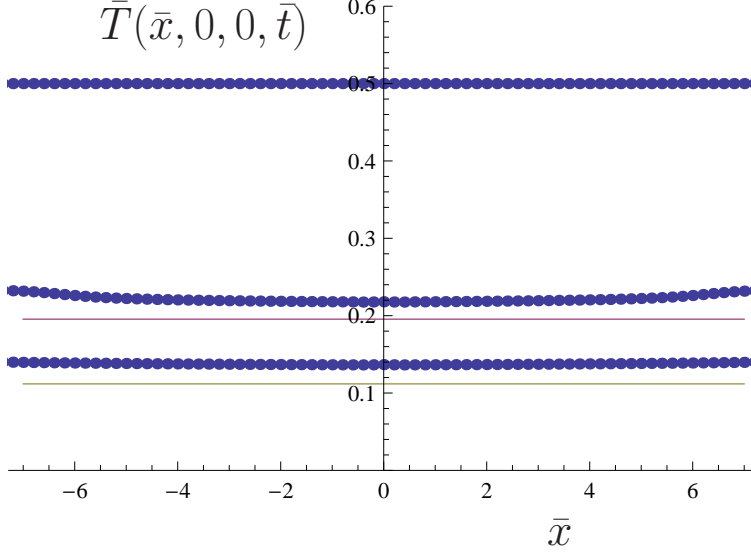


FIG. 7: This figure shows the evolution of the temperature profile in viscous hydrodynamics. The data points show the temperature $\bar{T}(\bar{x}, 0, 0, \bar{t})$ determined in a numerical simulation with $\bar{\alpha} = 0.1$ at several different times $\bar{t} = 0, 1.68, 2.70$. The lines are the result in ideal hydrodynamics.

time as compared to ideal hydrodynamics. In Fig. 6 we show $\delta\bar{t}_{cr}$ as a function of $\bar{\alpha}_n$ and λ . Ideal hydrodynamics predicts that $t_{cr} = \sqrt{\gamma}/(\lambda\omega_{\perp})$ with $\gamma = 2/3$. This result is correct in the limit $\lambda \ll 1$ up to higher order corrections in λ . Neglecting the effects of reheating the correction to the crossing time is [8]

$$\left(\frac{\delta t}{t}\right)_{cr} = 1.16 \frac{\langle \alpha_n \rangle}{(3N\lambda)^{1/3}} \frac{1}{(E_0/E_F)}, \quad (30)$$

where $\langle \alpha_n \rangle$ is the average of α_n over the initial density of the trap. The change in t_{cr} if reheating is included is shown in Fig. 6. In the upper panel we show the dependence of $\delta\bar{t}_{cr}$ on $\bar{\alpha}_n$. We observe that the effect remains linear if reheating is included, but that the sensitivity of $\delta\bar{t}_{cr}$ to $\bar{\alpha}_n$ is reduced by about a factor of 2. The lower panel shows that the correction factor depends on the geometry. If reheating is included then the sensitivity of $\delta\bar{t}_{cr}$ to the shear viscosity becomes very small in the limit of strongly deformed traps ($\lambda \rightarrow 0$). This is related to the fact that in this limit all internal energy is converted to transverse motion, irrespective of whether or not there is dissipation.

Fig. 7 shows the effect of reheating on the temperature profile of the cloud. The solid line shows the temperature profile at different times during the ideal evolution, and the data points come from a numerical simulation with $\bar{\alpha}_n = 0.1$. The increase in the average

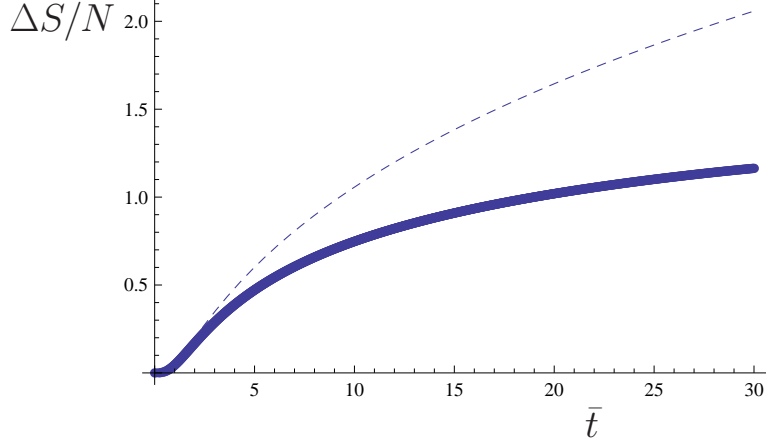


FIG. 8: This figure shows the evolution of the produced entropy per particle $\Delta S/N$ as a function of time. The thick line shows the result in a numerical simulation with $E_0/E_F = 1$ and $\bar{\alpha}_n = 0.1$ and the thin line is the entropy removed by the heat sink in the model discussed in Sect. IV.

temperature relative to the result in ideal hydrodynamics is due to reheating combined with a decrease in the expansion rate. In our simulation we have used a spatially constant α_n and the high temperature equation of state $P = nT$. In this case both the dissipated heat and the specific heat are proportional to the density. As a consequence the cloud remains isothermal to a fairly good accuracy.

Fig. 7 shows the change in the entropy per particle during the evolution of the system. The data points show the result of a simulation using an ideal gas equation of state with $E_0/E_F = 1$ and a shear viscosity $\bar{\eta} = \bar{\alpha}_n \bar{n}$ with $\bar{\alpha}_n = 0.1$. For the ideal gas equation of state we can compute the entropy using the Sackur-Tetrode formula. The dashed line shows the entropy absorbed by the the heat sink for a calculations with no reheating of the gas. In this case the produced entropy scales asymptotically as [8]

$$\frac{\Delta S}{N} \simeq 4 \left(\frac{2}{3}\right)^{1/3} \frac{\langle \bar{\alpha}_n \rangle}{(T_0/T_F)} (\omega_{\perp} t)^{1/3}. \quad (31)$$

The full simulation tracks the results without reheating very well for $(\omega_{\perp} t) \lesssim 3$. At later times the full simulation produces less entropy then the model without reheating. However, we still find that the total entropy continues to grow as $t \rightarrow \infty$. Numerically, we find that the asymptotic behavior is well described by $(\Delta S)/N \sim (\omega_{\perp} t)^{1/6}$.

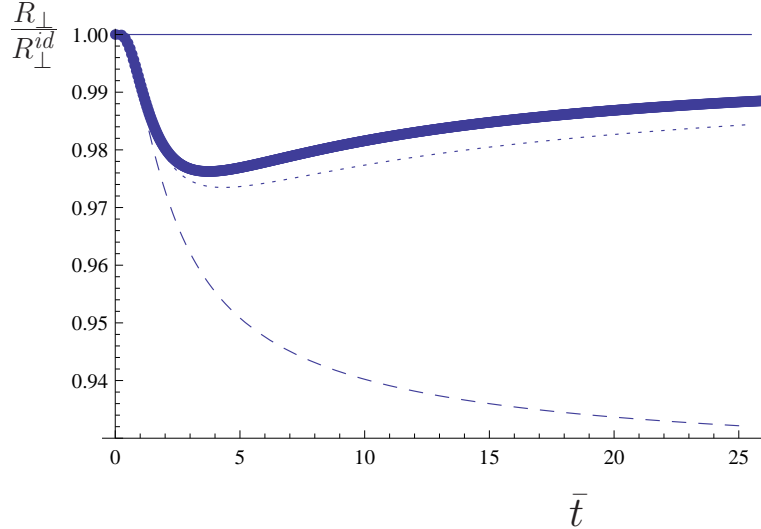


FIG. 9: This figure shows the ratio of the transverse scale factor in dissipative hydrodynamics over the result in ideal hydrodynamics. The data points are from a simulation with $\eta \sim n^2$ and $\langle \bar{\alpha}_n \rangle = 0.1$. The lines show the same calculations as in Fig. 4.

C. Dependence on the equation of state and the functional form of the shear viscosity

There are several arguments that indicate that the evolution of the system is not very sensitive to the equation of state $P(n, T)$ as long as the universal relation $P = \frac{2}{3}\mathcal{E}$ is satisfied. In Sect. IV we showed that the exact solution of Euler's equation is independent of the equation of state. We also showed that the equations of dissipative hydrodynamics given in equ. (23,24) are independent of the equation of state as long as the velocity field remains exactly linear. In this section we will study the dependence on the equation of state using numerical simulations of the complete hydrodynamic equations. We will compare the results obtained using the ideal gas equation of state $P = nT$ and the equation of state described in Appendix A. We consider a temperature $T = 0.25T_F$, close to the superfluid phase transition, where the deviation of the experimental equation of state from the ideal gas equation is largest. For the ideal gas equation of state we have $(E_0/E_F) = 3(T/T_F) = 0.6$. We choose $\bar{\alpha}_n = 0.06$ so that $\beta = 0.066$. For the experimental equation of state we find $E_0/E_F = 0.785$ and we set $\bar{\alpha}_n = 0.0785$ to keep β fixed. We find that the effect of the equation of state on the change in t_{cr} is smaller than the accuracy of our calculation,

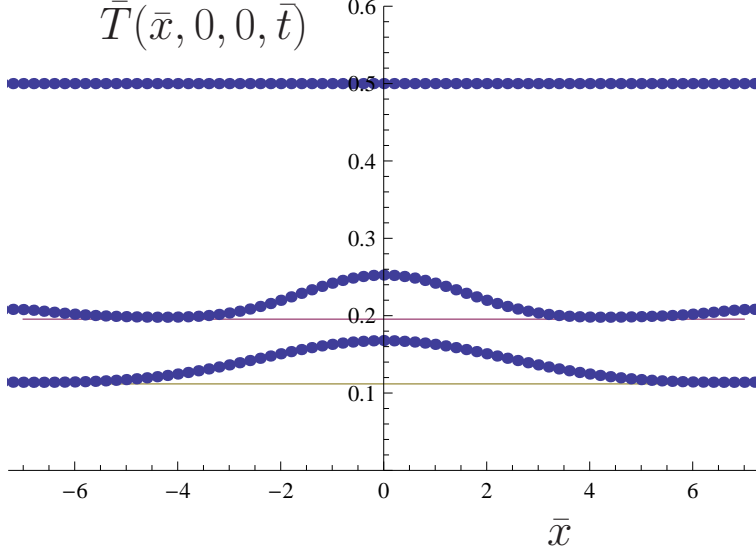


FIG. 10: This figure shows the evolution of the temperature profile in viscous hydrodynamics. The data points show the temperature $\bar{T}(\bar{x}, 0, 0, \bar{t})$ determined in a numerical simulation with $\eta \sim n^2$ and $\langle \bar{\alpha} \rangle = 0.1$ at several different times $\bar{t} = 0, 1.65, 2.66$. The lines are the result in ideal hydrodynamics.

$$(\delta t_{cr}(P^{id}) - \delta t_{cr}(P^{ex}))/t_{cr} < 10^{-3}.$$

We have also studied the dependence of dissipative effects on the functional form of the shear viscosity. The approximate solutions discussed in Sections IV and V suggest that dissipative effects depend only on the trap average $\langle \alpha_n \rangle$, see equ. (20). In the following we will test this idea by comparing calculations with $\alpha_n \sim const$, corresponding to $\eta \sim n$, and $\alpha_n \sim n/(mT)^{3/2}$, which implies $\eta \sim n^2/(mT)^{3/2}$. We write $\eta = \eta_2 n^2/(mT)^{3/2}$ and fix η_2 from $\langle \alpha_n \rangle$. For a Gaussian profile

$$\eta_2 = 24\pi^{3/2} \langle \alpha_n \rangle \left(\frac{T}{T_F} \right)^3. \quad (32)$$

Fig. 9 shows the evolution of the transverse radius for $\langle \bar{\alpha}_n \rangle = 0.1$. The lines are the same as in Fig. 4. We observe that the calculations with $\eta \sim n$ and $\eta \sim n^2$ are very similar for $(\omega_{\perp} t) \lesssim 3$. At later times the non-linear dependence of η on n leads to some extra acceleration. Fig. 10 shows the corresponding temperature profiles. We observe that for $\eta \sim n^2$ reheating takes place predominantly near the center of the cloud. This leads to an outward temperature gradient which is the source of the additional acceleration. Quantitatively, the difference

between the $\eta \sim n$ and $\eta \sim n^2$ is about 25%,

$$\frac{\delta t_{cr}(\eta \sim n) - \delta t_{cr}(\eta \sim n^2)}{\delta t_{cr}(\eta \sim n)} = 0.264. \quad (33)$$

D. Rotating solutions

In this section we study the time evolution of a rotating cloud. We take the initial velocity profile to be of the form $\vec{v} = \alpha \vec{\nabla}(xz)$ with $\alpha(0) = \omega_{rot} = 0.4\omega_z$ [20]. We have checked that the results are unaffected by taking the initial profile to be of the form $\vec{v} = \Omega \hat{y} \times \vec{x}$. The reason is that for a strongly deformed cloud the initial momentum density $\rho \vec{v}$ is essentially the same for irrotational or rigid initial conditions.

We determine the angle of the major axis and the aspect ratio of the cloud. The angle is related to the Gaussian radii by

$$\tan(2\theta) = \frac{2\langle xz \rangle}{\langle z^2 \rangle - \langle x^2 \rangle}, \quad (34)$$

and the aspect ratio is given by

$$A_R = \left\{ \frac{\langle x^2 \rangle + \langle z^2 \rangle + [(\langle z^2 \rangle - \langle x^2 \rangle)^2 + 4\langle xz \rangle^2]^{1/2}}{\langle x^2 \rangle + \langle z^2 \rangle - [(\langle z^2 \rangle - \langle x^2 \rangle)^2 + 4\langle xz \rangle^2]^{1/2}} \right\}^{1/2}. \quad (35)$$

Our results are shown in Fig. 11. The solid line is the result in ideal hydrodynamics. A good approximation to the evolution of the angle in ideal hydrodynamics is

$$\tan(2\theta) = -\frac{a\lambda^2 b_\perp^2 b_z^2}{b_\perp^2 - \lambda^2 b_z^2}, \quad (36)$$

where b_\perp, b_z are the scale parameters for the pure expansion (without rotation) and

$$a(t) \simeq \begin{cases} -\frac{2\omega_{rot}t}{\lambda^2} & \omega_\perp t \ll 1, \\ -\frac{\gamma\omega_{rot}}{\lambda^2\omega_\perp^2 t} & \omega_\perp t \gg 1, \end{cases} \quad (37)$$

with $\gamma = 2/3$. This result shows that the angle goes through 45 degrees at the same time at which the expanding system reaches an aspect ratio of 1.

Fig. 11 shows the time evolution of the angle and the aspect ratio. The solid line shows the result in ideal hydrodynamics, the dashed line shows the result in dissipative hydrodynamics neglecting reheating, and the data points are from a numerical simulation with $\bar{\eta} = \bar{\alpha}_n \bar{n}$ and $\bar{\alpha}_n = 0.1$. We observe that the effect of reheating in rotating clouds is similar to the effect in

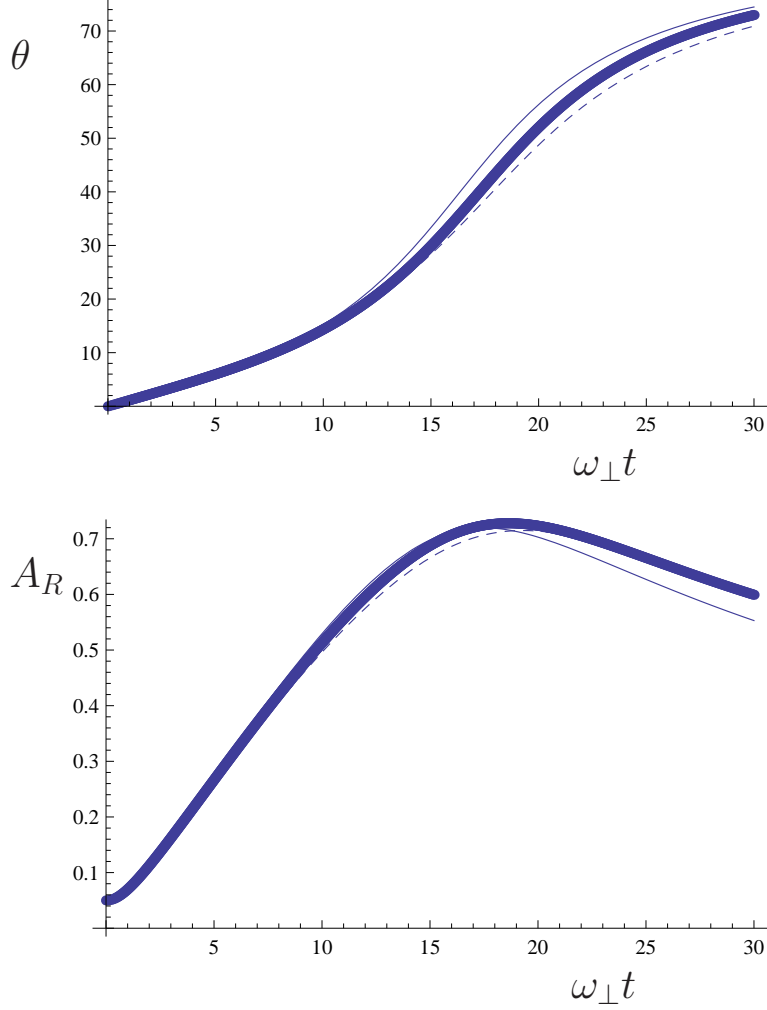


FIG. 11: This figure shows the time evolution of the angle (top panel) and the aspect ratio (bottom panel) of a rotating cloud as a function of time. The initial density profile is Gaussian, and the initial flow profile is an irrotational flow with $\omega_{rot} = 0.4\omega_z$. The thin line is the result in ideal hydrodynamics, the dashed line is the result in dissipative hydrodynamics with a heat sink, and the thick line is result of a numerical calculation with $\bar{\alpha} = 0.1$.

non-rotating systems. Reheating accelerates the system and reduces dissipative corrections. This effect can be quantified in terms of the time t_{45° at which the angle of the major axis passes through 45° (angular momentum conservation combined with the approximately irrotational nature of the flow implies that the aspect ratio never reaches the value 1). We find that, within the accuracy of our calculation, the dissipative correction to t_{45° is equal to the dissipative correction to the crossing time (see Sect. VIB), $\delta t_{45^\circ} = \delta t_{cr}$. This implies,

in particular, that earlier estimates of the shear viscosity based on calculations that do not take into account reheating have to be corrected by a factor ~ 2 [8, 22].

VII. CONCLUSIONS AND OUTLOOK

In this work we studied the expansion dynamics of a dilute Fermi gas at unitarity in the framework of dissipative hydrodynamics. Our main goal was to study whether one can extract the shear viscosity from expanding systems. This is not immediately obvious, because in an expanding system all internal energy is eventually converted into kinetic energy, irrespective of whether there is dissipation or not.

We find that shear viscosity does lead to characteristic effects in the expansion dynamics. Shear viscosity causes a characteristic curvature in the time evolution of the aspect ratio $A_R(t)$ of the cloud. In ideal hydrodynamics internal energy is converted to kinetic energy very quickly, over a time period $(\omega_\perp t) \lesssim 3$. After this time $A_R(t)$ is essentially linear. In dissipative hydrodynamics energy stored in the transverse motion is converted into longitudinal kinetic energy, and the longitudinal expansion takes place on a much longer time scale. As a result $A_R(t)$ exhibits a characteristic curvature at times as large as $(\omega_\perp t) \simeq \lambda^{-1} \simeq 25$. This effect was recently observed by Cao et al. [23], which shows that dissipative hydrodynamics is indeed valid at $(\omega_\perp t) \simeq 25$. This is a remarkable discovery, because during the evolution the density drops by a factor $\lambda^{-2} \sim 10^3$.

We also find that a quantitative description of the dependence of $A_R(t)$ and other observables on the shear viscosity has to include reheating. For a cloud with an aspect ratio of 25 the extracted shear viscosity is about a factor 2 too small if reheating is neglected. This affects the estimates presented in [8, 21, 22] but not the recent work of Cao et al. [23]. Reheating also does not affect estimates of the shear viscosity based on the damping of collective modes [18, 19].

We showed that a determination of the shear viscosity does not require an accurate knowledge of the equation of state $P(n, T)$. The only important aspect of the equation of state is the universal relation $P = \frac{2}{3}\mathcal{E}$. We also studied the dependence of viscous effects on the functional form of $\eta(n, T)$. We find that to first approximation the expansion dynamics constrains the cloud average of the shear viscosity. In this approximation the universal function $\alpha_n(mT/n^{2/3})$ can be determined by extracting $\langle \alpha_n \rangle$ as a function of T/T_F from

data, and then inverting equ. (21). This only requires knowledge of the initial density profile. The result can be used as input for a more accurate determination based on full hydrodynamics.

There are several issues that remain to be studied. The most important problem has to do with the breakdown of hydrodynamics in the dilute corona of the cloud. In the low density, high temperature limit the shear viscosity can be reliably computed. The result shows that the shear viscosity is independent of the density, $\eta \sim (mT)^{3/2}$. This implies that the total amount of heat dissipated by the dilute tail of the density distribution is infinite. We have previously argued that this problem can be resolved by taking into account the fact that the dissipative contribution to the stress tensor relaxes to the Navier-Stokes form on a time scale which is proportional to the density of the system [8, 29]. In kinetic theory we expect that $\tau_R \partial_t (\delta \Pi_{ij}) = (\eta \sigma_{ij} - \delta \Pi_{ij})$ where the relaxation time is given by $\tau_R = \eta / (nT)$. This implies that in the dense regime the shear viscosity relaxes to its equilibrium value on a time scale that is fast compared to the time scale of the hydrodynamic expansion, but in the dilute regime dissipation is governed by an effective viscosity which is proportional to the density.

This idea can be implemented by using an effective $\langle \alpha_n \rangle$ in solving the equations of dissipative hydrodynamics [8, 23]. It is clearly preferable, however, to include the effects of finite relaxation time by including higher derivative terms in the equations of dissipative fluid dynamics (this is known as 2nd order, or Burnett, hydrodynamics), or by coupling the hydrodynamic description to kinetic theory.

Acknowledgments: This work was supported in parts by the US Department of Energy grant DE-FG02-03ER41260. We would like to thank Clifford Chafin and John Thomas for useful discussions and John Blondin for help with VH1.

Appendix A: Equation of state

In this appendix we describe a parameterization of the equation of state in the normal phase. The equation of state has been studied experimentally [30–32], using quantum Monte Carlo simulations [33–35], and many-body theory [36, 37]. Here we follow the recent work of Nascimbene et al. [31] and write

$$P(\mu, T) = P_1(\mu, T)h(\zeta), \tag{A1}$$

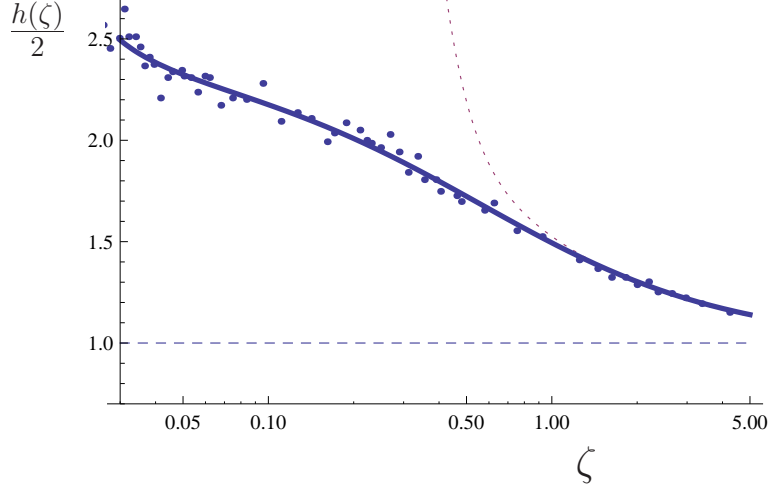


FIG. 12: Equation of state of the unitary Fermi gas in the normal phase. In this figure we show the function $h(\zeta)$, where ζ is the fugacity. The data points are from Nascimbene et al., the thick solid line shows the parameterization discussed in the text, the dashed line is the non-interacting gas result $h = 1$, and the dotted line shows the second order Virial expansion.

where $P_1(\mu, T)$ is the ideal gas equation of state of a single species non-relativistic Fermi gas

$$P_1(\mu, T) = -T\lambda_{dB}^{-3}Li_{5/2}(-\zeta^{-1}), \quad (\text{A2})$$

and $\lambda_{dB} = [(2\pi)/(mT)]^{1/2}$ is the de Broglie wave length. Here, $Li_\alpha(x)$ is the Polylogarithm function, and $\zeta = \exp(-\mu/T)$ is the fugacity. We parameterize $h(\zeta)$ as

$$\frac{h(\zeta)}{2} = \frac{\zeta^2 + c_1\zeta + c_2}{\zeta^2 + c_3\zeta + c_4}, \quad (\text{A3})$$

and determine the parameters c_i from a fit to the data of Nascimbene et al. [31]. This parameterization is motivated by the fact that the data for $\zeta > 1$ is very well described by the Virial expansion $h(\zeta)/2 = 1 + b_2/\zeta + b_3/\zeta^2 + O(1/\zeta^3)$. At unitarity $b_2 = 1/\sqrt{2}$ and $b_3 = \frac{1}{8} - 0.355 = 0.23$. The value of $h(\zeta)$ at zero fugacity is related to the Bertsch parameter $\xi = \mu/E_F$. Using $\xi \simeq 0.4$ we have $h(0)/2 = \xi^{-3/2} \simeq 3.8$. A fit for fugacities in the range $\zeta \in [0.03, 5]$ gives

$$c_1 = 1.3543, \quad c_2 = -0.0174, \quad c_3 = 0.5724, \quad c_4 = -0.0084. \quad (\text{A4})$$

We compare the data to our fit and the Virial expansion in Fig. 12. From the pressure we can determine other thermodynamic quantities. The density and entropy density are given

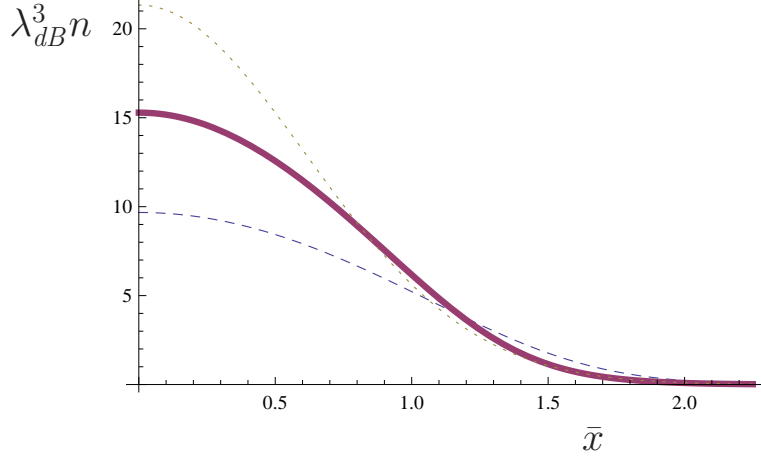


FIG. 13: Density of a trapped Fermi gas in the local density approximation at a temperature $T/T_F = 0.25$, slightly above the critical temperature. The thick line is the result based on the equation of state from Nascimbene et al., the dashed line is the result for a free gas, and the dotted line shows the result using the equation of state in the high temperature limit.

by

$$n(\mu, T) = \lambda_{dB}^{-3} g(\zeta), \quad s(\mu, T) = \lambda_{dB}^{-3} k(\zeta), \quad (\text{A5})$$

with

$$g(\zeta) = -Li_{3/2}(-\zeta^{-1})h(\zeta) + \zeta Li_{5/2}(-\zeta^{-1})h'(\zeta), \quad (\text{A6})$$

$$k(\zeta) = -\left(\log(\zeta)Li_{3/2}(-\zeta^{-1}) + \frac{5}{2}Li_{5/2}(-\zeta^{-1})\right)h(\zeta) + \log(\zeta)Li_{5/2}(-\zeta^{-1})h'(\zeta). \quad (\text{A7})$$

In a trapped system we use the local density approximation $n(x) = n(\mu(x), T)$ with $\mu(x) = \mu - V(x)$ where $V(x)$ is the trapping potential. This determines the density profile if the temperature and the chemical potential (or the fugacity) at the center of the trap are given. In practice we usually specify the temperature and the total number of particles. The particle number defines a temperature scale $T_F = (3N)^{1/3}\bar{\omega}$, where $\bar{\omega} = (\omega_x\omega_y\omega_z)^{1/3}$ is the geometric mean of the trap frequencies. Given T/T_F the fugacity ζ_0 at the center of the trap is determined by the condition

$$\frac{3}{(2\pi)^{3/2}} \left(\frac{T}{T_F}\right)^3 \int d^3x g\left(\zeta_0 \exp\left(\frac{x^2}{2}\right)\right) \equiv 1. \quad (\text{A8})$$

This equation has to be solved numerically. In the high temperature limit $\zeta_0 = 6(T/T_F)^3$. In Fig. 13 we show the density profile at $T/T_F = 0.25$. We show the exact density, the

density of a free gas, and the high temperature (Gaussian) approximation. The effects of quantum degeneracy decrease the central density, whereas interactions increase the density. The two effects partially cancel and the exact density is about 50% larger than the Gaussian approximation.

Once the initial density and pressure have been determined the equations of fluid dynamics fix the evolution of P and n . The equation of state is needed in order to compute other thermodynamic quantities like the temperature and the chemical potential [38]. The fugacity can be computed from

$$\frac{2}{(2\pi)^{3/2}} \left(\frac{mP}{n^{5/3}} \right)^{3/2} = 2 \frac{f(\zeta)^{3/2}}{[-\zeta f'(\zeta)]^{5/2}} \equiv F(\zeta), \quad (\text{A9})$$

where $f(\zeta) = -Li_{5/2}(-\zeta^{-1})h(\zeta)$. Equ. (A9) implies that

$$\zeta = F^{-1} \left(\frac{2}{(2\pi)^{3/2}} \frac{m^{3/2} P^{3/2}}{n^{5/2}} \right). \quad (\text{A10})$$

In general, $F^{-1}(y)$ has to be computed numerically. In the high temperature limit $F^{-1}(y) \simeq y$. Once the fugacity is known the temperature can be computed from

$$T = -\frac{\zeta f'(\zeta) P}{f(\zeta) n}. \quad (\text{A11})$$

In the high temperature limit $f(\zeta) \simeq 2/\zeta$ which implies $\zeta f'(\zeta)/f(\zeta) \simeq -1$ and $T = P/n$.

-
- [1] I. Bloch, J. Dalibard, W. Zwerger, Rev. Mod. Phys. **80**, 885 (2008) [arXiv:0704.2511].
 - [2] S. Giorgini, L. P. Pitaevskii, S. Stringari, Rev. Mod. Phys. **80** 1215 (2008) [arXiv:0706.3360].
 - [3] C. Chin, R. Grimm, P. Julienne, E. Tiesinga Rev. Mod. Phys. **82** 1225 (2010) [arXiv:0812.1496].
 - [4] K. M. O'Hara, S. L. Hemmer, M. E. Gehm, S. R. Granade, J. E. Thomas, Science Vol. 298, No. **5601**, 2179 (2002) [cond-mat/0212463].
 - [5] T. Schäfer and D. Teaney, Rept. Prog. Phys. **72**, 126001 (2009) [arXiv:0904.3107 [hep-ph]].
 - [6] D. T. Son, Phys. Rev. Lett. **98**, 020604 (2007) [arXiv:cond-mat/0511721].
 - [7] M. A. Escobedo, M. Mannarelli and C. Manuel, Phys. Rev. A **79**, 063623 (2009) [arXiv:0904.3023 [cond-mat.quant-gas]].
 - [8] T. Schäfer and C. Chafin, arXiv:0912.4236 [cond-mat.quant-gas].

- [9] M. Braby, J. Chao and T. Schäfer, arXiv:1003.2601 [cond-mat.quant-gas].
- [10] G. M. Bruun, H. Smith, Phys. Rev. A **72**, 043605 (2005) [cond-mat/0504734].
- [11] G. M. Bruun, H. Smith, Phys. Rev. A **75**, 043612 (2007) [cond-mat/0612460].
- [12] G. Rupak and T. Schäfer, Phys. Rev. A **76**, 053607 (2007) [arXiv:0707.1520 [cond-mat.other]].
- [13] E. Taylor and M. Randeria, arXiv:1002.0869 [cond-mat.quant-gas].
- [14] T. Enss, R. Haussmann and W. Zwerger, arXiv:1008.0007 [cond-mat.quant-gas].
- [15] P. Danielewicz and M. Gyulassy, Phys. Rev. D **31**, 53 (1985).
- [16] P. Kovtun, D. T. Son and A. O. Starinets, Phys. Rev. Lett. **94**, 111601 (2005) [arXiv:hep-th/0405231].
- [17] B. A. Gelman, E. V. Shuryak, and I. Zahed, Phys. Rev. A **72**, 043601 (2005) [nucl-th/0410067].
- [18] T. Schäfer, Phys. Rev. A **76**, 063618 (2007) [arXiv:cond-mat/0701251].
- [19] A. Turlapov, J. Kinast, B. Clancy, L. Luo, J. Joseph, J. E. Thomas, J. Low Temp. Phys. **150**, 567 (2008) [arXiv:0707.2574].
- [20] B. Clancy, L. Luo, J. E. Thomas Phys. Rev. Lett. **99** 140401 (2007) [arXiv:0705.2782 [cond-mat.other]].
- [21] B. Clancy, Ph.D. Thesis, Duke University (2008).
- [22] J. E. Thomas, Nucl. Phys. A **830**, 665C (2009).
- [23] C. Cao, E. Elliott, J. Joseph, H. Wu, J. Petricka, T. Schäfer, J. E. Thomas, arXiv:1007.2625 [cond-mat.quant-gas].
- [24] C. Menotti, P. Pedri, S. Stringari, Phys. Rev. Lett. **89**, 250402 (2002) [cond-mat/0208150].
- [25] M. Edwards, C. W. Clark, P. Pedri, L. Pitaevskii, S. Stringari, Phys. Rev. Lett. **88** 070405 (2002).
- [26] J. M. Blondin, E. A. Lufkin, Astrophys. J. Supp. Ser. **88**, 589 (1993).
- [27] P. R. Woodward, P. Colella, J. Comp. Phys. **54**, 115 (1984).
- [28] P. Colella, P. R. Woodward, J. Comp. Phys. **54**, 174 (1984).
- [29] G. M. Bruun, H. Smith Phys. Rev. A **76**, 045602 (2007) [arXiv:0709.1617].
- [30] L. Luo, J. E. Thomas, J. Low Temp. Phys. **154**, 1 (2009), [arXiv:0811.1159[cond-mat.other]].
- [31] S. Nascimbene, N. Navon, K. Jiang, F. Chevy, C Salomon, Nature **463**, 1057 (2010) [arXiv:0911.0747[cond-mat.quant-gas]].
- [32] M. Horikoshi, S. Nakajima, M. Ueda, T. Mukaiyama, Science Vol. 327, No. **5964**, 442 (2010).
- [33] D. Lee and T. Schäfer, Phys. Rev. C **73**, 015202 (2006) [arXiv:nucl-th/0509018].

- [34] E. Burovski, N. Prokof'ev, B. Svistunov, M. Troyer, Phys. Rev. Lett. **96**, 160402 (2006) [cond-mat/0602224].
- [35] A. Bulgac, J. E. Drut and P. Magierski, Phys. Rev. A **78**, 023625 (2008) [arXiv:0803.3238 [cond-mat.stat-mech]].
- [36] Q. Chen, J. Stajic, S. Tan, K. Levin, Phys. Rep. **412**, 1 (2005).
- [37] R. Haussmann, W. Rantner, S. Cerrito, W. Zwerger, Phys. Rev. A **75**, 23610 (2007) [arXiv:cond-mat/0608282].
- [38] If thermal conductivity is included then the temperature has to be determined at each step in the hydrodynamic evolution in order to compute the energy current.